

# Determining colours of NGC 1073

Sjoerd Hardeman and Thijs Coenen

University of Amsterdam

Faculty of Science



# Determining colours of NGC 1073

Sjoerd Hardeman and Thijs Coenen

University of Amsterdam

Faculty of Science

December 24, 2005

## **Abstract**

We have observed NGC 1073 at the Mercator telescope using filters. From this data we have obtained colours from different parts of the galaxy. The results show a difference in colour between the bulge and the spiral arms, especially near areas with star formation. Comparing the observations to the Starburst99 stellar population synthesis model we found an area with very young stars. Also, comparing our observations with this model tentatively suggest that the bar is older than the spiral arms.

## **Acknowledgements**

We would like to thanks everybody who helped us along. We want to thank Diego Altamirano for being a good guide at La Palma and being patient with us. We also want to thank Wim de Meester for his hospitality and support during the observation run. Rens Waters was a great in support writing the report, therefore we would like to thank him. Finally, we want to thank all the students participating in this course for a great time and all the work they did for us.

# Contents

<b>1</b>	<b>Introduction: Stellar populations and galaxy formation</b>	<b>3</b>
1.1	Stellar populations . . . . .	3
1.2	Stellar populations in spiral galaxies . . . . .	5
<b>2</b>	<b>Theory of stellar synthesis</b>	<b>6</b>
2.1	Stellar population synthesis . . . . .	6
2.2	Stellar emission . . . . .	7
2.3	Calculating the total spectrum and colours . . . . .	8
<b>3</b>	<b>Observations</b>	<b>11</b>
3.1	Selection of targets . . . . .	11
3.2	Site and Telescope . . . . .	11
3.2.1	CCD Camera . . . . .	11
3.2.2	Filters . . . . .	11
3.3	Data collected . . . . .	13
3.4	Conditions . . . . .	14
3.5	Data reduction and calibrations . . . . .	14
<b>4</b>	<b>Results</b>	<b>18</b>
4.1	Quantitative data form the galaxy . . . . .	18
4.2	Images . . . . .	22
4.3	Description of observations . . . . .	22
4.4	Comparing colours to the Starburst99 model . . . . .	26
<b>5</b>	<b>Conclusions</b>	<b>29</b>
<b>6</b>	<b>Discussion</b>	<b>30</b>

# 1 Introduction: Stellar populations and galaxy formation

An interesting question in the formation of the universe is the actual formation of galaxies. There is still a lot that is not known about these objects. Questions like when galaxy formation started, if that date is before or after the appearance of the first stars and questions about galaxy evolution remain unanswered.

To study galaxy formation history, you need a lot of data. Information on young galaxies for example, as obtained by the Hubble deep field. Also helpful is information on their gas content, which you can try to get from 21cm surveys. To study kinematics within galaxies, which can tell you a lot about the mass distribution, you need information on stellar orbits. Finally it is helpful to know the stellar formation history, and try to identify starburst periods [14].

This last subject will be the scope of our research. Before we continue, let's pause and wonder why it is interesting. Actually, there are several questions you can answer studying stellar populations. First of all, you can isolate periods of active star formation. These starburst periods, as they are known, are normally caused by disruptions of the galaxy, often by interaction with other galaxies. Active formation is also omnipresent in young galaxies, so tracking periods of active star formation can give you insight in the history of your galaxy [8].

Furthermore, star formation rates contain information about the mass fraction of gas in a galaxy. A higher mass fraction can result in higher star formation rates. Of course star formation is also determined by the distribution of gas through the galaxy. Although this information can also be obtained by other methods, this method has the advantage of working up to large distances, and giving an additional method of deriving an interesting quantity. The question on star formation is especially interesting, as older galaxies which are still rich in gas often still present infalling gas clouds [7, 15].

Let's now focus somewhat more on our research. We are not going to try to answer questions like those above, as they need input from a large number of galaxies which we do not have. We can however try to get stellar population information of one galaxy, and see if we can learn anything from the result. Before we proceed, we will first discuss some general theory about stellar populations.

## 1.1 Stellar populations

In a normal spiral galaxy, stars are continuously formed. This formation takes place in collapsing clouds of gas and dust, seen as dark clouds on most visual images. When stars in such a cloud start shining, they heat up the gas, dispersing it and thereby ending the stellar formation. In this process, the clouds show up as beautiful coloured emission and reflection nebulae on your CCD. A tracer for stellar formation are the HII regions. These regions are formed when a massive star is formed, ionising the gas around it. Recombination into the first excited state of hydrogen produces radiation



at 6563 Å, seen as red light.

Star formation produces a more or less fixed amount of lightweight stars per heavy star. Research by Salpeter has given us an initial mass function (IMF), based on local observations, stating the mass distribution of star formation[12]

$$N^*(M) = N_0 M^x \quad (1)$$

$$\begin{aligned} M &\geq 0.5 M_\odot & x &= -2.35 \\ M &\leq 0.5 M_\odot & x &= 0 \end{aligned}$$

Assuming that this relation also holds in other galaxies, you can calculate the mass fraction of stars of a different age at formation, given the total formation rate.

Another ingredient needed is the life span of a star, as we need the mass fraction of stars of a certain age, not at formation. For this we need a relation telling us how long a star will live having a specified mass  $M$ . However, this is not a problem since this relation is known from stellar theory. As a first approximation you can use the main sequence lifetime. This lifetime is obtained from the mass-luminosity relation and the assumption that main sequence stars have a same percentage of nuclear fuel available. We use a mass-luminosity relation of  $L \propto M^{3.5}$ , which is an accepted value for most of the main sequence [2]. The relation then becomes

$$t_{max} = 10^{10} * \left( \frac{M}{M_\odot} \right)^{-2.5} \text{ yrs} \quad (2)$$

In which  $t_{max}$  is the lifetime at which a star leaves the main sequence. Better approximations include the post-main sequence life of a star, including the vastly changed properties of its giant state. This is especially important for older stellar populations, where most of the flux is emitted by the giants. Although the model we use accounts for this, it is a far from trivial subject we will not discuss in our report.

Combining these equations you can calculate the total number of stars of mass  $M$  in your galaxy. To do this you need to calculate the following convolution integral:

$$N_*(M_1 - M_2) = \int_t \int_{M_1}^{M_2} N_*(M)|_{t_{0,*}} \times f(M, t_{0,*} - t') dM dt' \quad (3)$$

This equation relates  $N_*(M)|_{t_{0,*}}$ , which contains the star formation history and  $f(M, t)$  the mass/age equation. The mass/age equation is for example the one in equation 2, normalised to 1 at  $t = 0$ . It is actually a probability function of a star of mass  $M$  still being alive at age  $t$ . Assuming the spread of this probability being small, this function can be replaced by the step function

$$f(M, t) = \Theta(t_{max}(M) - t)$$

in which  $\Theta(x)$  is the step function.

This essentially is the information you are after. Knowing the distribution of stellar masses, you can reconstruct the formation history of the galaxy. This mass distribution can be obtained by several methods, including integrated spectra and colours of integrated areas full of stars.

## 1.2 Stellar populations in spiral galaxies

To study the star formation history of a galaxy, it is interesting to know about the different stellar populations that are present. In this paper, we try to obtain that information from observations with a set of filters from NGC 1073. In section 3 we explain why we chose this galaxy. The images from these filters can be translated into differences in brightness in the different bands that can pass the used filters. That information can be translated into information about stellar populations using stellar synthesis models. We will try to fit such a model to our data, the fit parameters being the age distribution of the stars in the examined fraction of the galaxy.

In spiral galaxies you can identify a bulge and a disk. The bulge is more or less elliptical in shape, is quite bright due to the high density of stars, and has generally an old population of stars. We expect to see this in our colour data by a relatively large flux in the low frequency filters compared to the high frequency filters.

The spiral arms are formed due to active star formation. Therefore, we expect to see a much younger population in the disk, especially near the spiral arms [5]. This is translated into a much bluer colour of the disk. The areas of actual stellar formation may also show a large red colour. This is because the hot, young stars ionise the gas around it. When recombining, hydrogen emits at a wavelength of 6563 Å. These areas are clearly identified as red spots in other galaxies. However, as we haven't used the R filter, the filter around this frequency, we can not use this feature.

Suggested is a close resemblance in star formation and spiral galaxy structure [10]. The bulge is considered to have formed in a star burst period early in the galaxy formation, and now not to host star formation anymore [13]. Star formation is still present in the disk, where density waves form the onset of stellar formation in the spiral arms. Therefore, there is a close relation in the running of those density waves and the distribution of young stars.

In the remainder of this paper, we will first describe the Mercator telescope, the telescope we used to take the images. Following, we will explain how we calibrated the data. After that, we will use the data to obtain colour information of NGC 1073, the examined galaxy. We will then try to fit a model to these colours, giving an estimate of the age distribution of stars in the galaxy. This model will be the Starburst99 stellar population synthesis model, of which we will provide a short description. Finally we will discuss the results we have obtained.

## 2 Theory of stellar synthesis

In this section we will first describe how an integrated flux is formed from different emitting sources. After that we will look more closely on one of these contributions: the stellar flux. We will see that this problem does have unique solutions, provided you know the exact spectrum. Finally we will use the results obtained in this chapter and calculate colours for known configurations of stars. These configurations can then be used to fit our measurements.

As shown in section 1, the stellar populations is what you are after. What we are thus looking for is a method of computing the stellar populations from a flux distribution, which can be measured. Assuming that for each set of properties a star has a unique spectrum, this problem is intrinsically solvable. This because we want to convert a continuous flux distribution to a continuous mass distribution. Therefore, for all variables there is a boundary condition. In our case, however, we only have four boundary conditions, being the four filter fluxes we measured. Therefore, we can only determine four groups of populations, assuming these groups cover the entire problem. Of course this will lead to a degenerate set of eigenvalues, thereby making the actual results model dependent. As we will see later, there is also another degeneracy troubling us, as there is an overlap in the function describing the stellar flux between metallicity and stellar mass.

### 2.1 Stellar population synthesis

From the results in section 1, it is actually a simple exercise to calculate the total flux as a function of wavelength. All you need to do is add up all the stars weighted with their individual fluxes.

$$\mathcal{F}_{tot}(\nu) = \sum_{stars} \mathcal{F}_*(\nu) + \mathcal{F}_{nebulas} \quad (4)$$

This is the total flux for a known number of stars with flux  $\mathcal{F}_*(\nu)$ , which in principle is known from stellar theory. This is, however, not a trivial problem, as we shall see in section 2.2. This function gives an absolute flux, and therefore also depends on distance and number of stars. If you are not interested in these properties, only the shape of the spectrum matters and the above formula should be multiplied by an arbitrary factor. The flux also contains emission from interstellar gas, which is often present, especially in young open clusters. Not included is possible emission from compact objects. This because it is only important at short (X-ray) wavelengths or in the presence of an active galactic nucleus. We will justify neglecting this flux later in this section.

Of course this is not the whole story, as the galaxy emission is the sum of the stellar and non stellar emission, corrected for intra-galaxy extinction. Both the non stellar emission and the extinction we've taken to be zero, which is not justified. Let's first address the extinction. This is a difficult problem, as extinction is a strong function of

position in the galaxy and metallicity. To make matters simple for us, we've decided to use a face on spiral. Such a galaxy has on average a low column density: the integrated path length the light has to travel through the galaxy is short. Therefore, we assume we may neglect extinction. We think this is a reasonable assumption, except for star forming regions where the column densities are large even for short columns. However, as stellar nurseries are on average dominated by bright, blue stars, you can choose to correct the spectra of these stars for extinction, and also add the extra nebula emission (H- $\alpha$  emission and NII emission, for example) to their spectra. This latter step will solve an important contribution of the non-stellar emission in a galaxy.

Another source of non stellar emission may be a central black hole accreting mass. As we are unaware of large fluxes being emitted by the bulge of NGC 1073, we assume that there is no black hole accreting large quantities of mass, and neglect its possible contribution. For other sources (Seyfert galaxies, quasars) this is a tricky problem that needs to be addressed. This needs to be done by a case by case scenario, especially adapted for the galaxy you are observing.

## 2.2 Stellar emission

In the previous section we've discussed how you can calculate a total flux, given the flux of all individual stars and other contributing sources. While we have discussed (and then neglected) the emission of non stellar sources, we've skipped the most difficult question: that of stellar emission. To be able to calculate the total emission using equation 4, we do need an expression for  $\mathcal{F}_*(\nu)$ . While extended theory has developed on this subject, it is so important that we will summarise some important aspects here.

The main difficulty of calculating  $\mathcal{F}_*(\nu)$  is that it depends on a lot of non trivial constants. Consider  $\mathcal{F}_*(\nu)$  to be a function of age, metallicity, mass and surrounding material (remember that we've added nebular effects to the stellar emission). Although the function is complex, it is invertible if measured closely enough. In other words: if you know the spectrum of a star in enough detail, you can in principle calculate all the values this spectrum depends on. While we will not discuss stellar spectra fully, we will consider each aspect qualitatively.

Age has the most important effect on the spectrum of a star. While the spectrum of a star does not change a lot on the main sequence track, in later stadia of its life it changes completely. The spectrum of a red giant is completely different from any main sequence star. First of all red giants are rather large for their temperature, thereby emitting a large flux. As they are generally cool, this flux is emitted in the low frequency part of the spectrum. Therefore, supergiants often have greater influence on the low frequency part of the spectrum than light, cool stars. This effect will be of most importance to us. Second, as the star grows the surface gravity drops, giving rise to a stellar wind. This will cause the spectral lines to change shape. Although it is an important subject, it will not be of great importance to us as we

do not look at spectral lines. However, if such stars having particular deep spectral lines dominate your spectrum, you lose a noticeable amount of flux in these lines, which should be taken into account. The fact that we cannot observe spectral lines is also the main reason we have to solve a degenerate problem. A source with a large number of spectral lines has to emit all the flux which is not emitted in those lines at other frequencies. Theory tells you that this flux is emitted at longer wavelengths, thus reddening the spectrum. Therefore, we cannot distinguish between a spectrum having a large number of spectral lines or a redder spectrum.

Second, you need to consider metallicity. Metals often have a large number of electrons, allowing for a large number of excited states. Therefore, metals bring numerous spectral lines. As metallicity rises, these spectral lines become deeper, taking away flux in their lines. In areas of the spectrum with a high number of metal lines, a rising metallicity will result in a significantly lower flux. In order to calculate stellar spectra correctly, you should therefore consider metallicity. As explained in the previous paragraph, this will also give rise to degeneracy. As metals produce spectral lines, they tend to redden the colours, in the same way as an ageing population reddens. We will therefore not be able to distinguish between metallicity and age.

Another, equally important property of metals is that they are the building blocks of dust. In low metallicity galaxies there is less dust. Although we've chosen to neglect dust, we are taking into account star forming regions. As opacity is also a strong function of dust content, to calculate this contribution correctly requires knowledge of the metallicity of the gas.

Finally we need to consider that a stellar population is made up of different kinds of stars. After taking out metallicity and age, these differences only depend on mass. This can be done using mass-luminosity and mass-temperature relations. The life sequence of a star is of course also mass dependent, but as this is closely related with the moment of star formation this is most easily accounted for there.

A stellar spectrum will differ significantly for different masses, the theory behind that being complex. In general differences can be traced back to higher temperatures leading to a different ionisation fraction, thereby making different spectral lines important. On top of that there's the temperature-dependent Planck distribution, determining roughly the overall shape of a spectrum. More information on stellar spectra can be found in [3, 16, 1]

## 2.3 Calculating the total spectrum and colours

From the previous information it is now possible to calculate the total spectrum, at least if you know all the variables. As is clear from the text this is a far from trivial exercise, requiring you to keep track of stellar formation and evolution histories. On top of that, you should take care to consider metallicity correctly.

Assuming you can do all this, you end up with a total spectrum emitted by the set of stars under consideration. However, the telescope we used doesn't have a

spectrograph, so we need to look at the frequency dependent flux in a different way. This can be done by photometry using filters. Filters allow only a relatively small band of frequencies pass. Using different filters at varying frequency regions you can then reconstruct the overall shape of the spectrum. Before we calculate colours from a spectrum we first deal with some terminology. The amount of flux passing through your filter determines a magnitude, of course after proper calibration. A magnitude is therefore a measure of the brightness of your object in a certain frequency range. The difference between two magnitudes gives you a colour.

To make matters more complicated, transmission curves from a filter are seldom easy functions (see image 3 for the transmission curves of the filters used by us). Therefore you cannot suffice by adding up all the flux in a certain frequency range, but you have to calculate a convolution integral

$$IBF = \int_0^\infty \mathcal{F}_*(\nu)T(\nu)d\nu \quad (5)$$

In this equation  $T(\nu)$  is the function for the transmission curve of a filter. This integral gives you the total flux which converts into a magnitude in the usual way by taking the logarithm. The final equation of calculating colours is then

$$M_1 - M_2 = 2.5 \log_{10} \left( \frac{F_1}{F_2} * \frac{\text{cal}_2}{\text{cal}_1} \right) \quad (6)$$

which is only dependent on the relative fraction of flux in each colour channel. The  $\text{cal}_n$  are the necessary calibrator factors: the zero point value and the atmospheric extinction correction. After doing all this math, we are in principle able to calculate

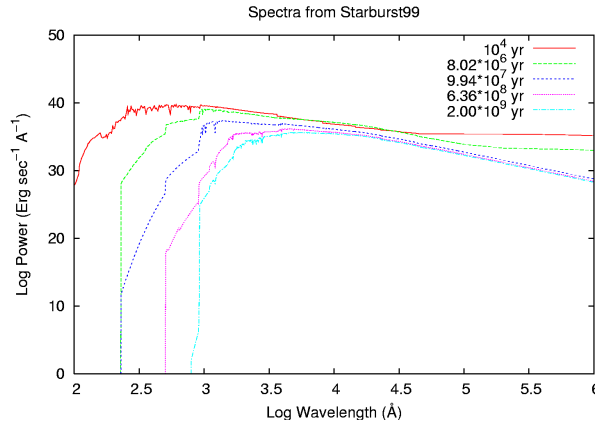


Figure 1: Synthetic stellar population spectra as calculated by Starburst99. The reddening of an ageing population is clearly seen.

colours for a given set of stars formed by a specified formation history. To do this,

we actually use a computer program, Starburst99 [9, 17]. This program can calculate so called stellar population synthesis models. These programs calculate a synthetic stellar population, based on stellar formation history and stellar theory. From this population quantities like spectra and colours can be calculated. In figure 1 is an example of Starburst99 output.

Using the results from this program you can try to fit the colours you measured to colours calculated by the program. The fit parameters are then metallicity and age distribution, two important quantities for tracking down stellar formation histories in galaxies.

## 3 Observations

In this section we will describe why we chose NGC 1073 as our source. We will also go through the steps we took to clean up our raw data and some of the analyses we performed on our dataset.

### 3.1 Selection of targets

The goal of our observational project was to compare the colours of different parts of a galaxy and try to find ages for the different stellar populations. We wanted a spiral galaxy because it has a well defined bulge and spiral arms. Also, these galaxies still form stars. To minimise the extinction within the galaxy we chose a face on spiral. Furthermore, we wanted a galaxy that fitted our CCD, so it should be slightly smaller than  $6.5' \times 6.5'$ . We chose NGC 1073 for practical reasons, it would be close to the zenith when we were at the Mercator observatory in La Palma making it easily observable.

### 3.2 Site and Telescope

All observations were made with the Mercator telescope situated at the Observatorio Roque de los Muchachos[4]. This observatory is at the island La Palma, one of the Canary Islands, at 28d 45' 44" N latitude and 17d 52' 42" W longitude at an altitude of 2333 m. The Mercator telescope is operated by the Instituut voor Sterrenkunde "Katholieke Universiteit Leuven" (Belgium). It is a mirror telescope with a primary mirror of 1200 mm with a focal length of 3360 mm and a secondary mirror of 305 mm with a focal length of 996 mm. The telescope can be used with either the Merope CCD camera or the P7 photometer. There are 9 photometric filters available: *UG*, *BG1*, *BG*, *BG1*, *VG1*, *VG*, *GG*, *RG* and *IC*. In the next sections the CCD camera and filters will be discussed.

#### 3.2.1 CCD Camera

The Merope CCD camera used at the Mercator telescope has a total field of view (FOV) of  $6.5' \times 6.5'$  with a sampling of  $0.19''$ . The camera chip is a  $2k \times 2k$  EEV 42-40 thinned and back-side illuminated device of grade 1. It is cooled with liquid nitrogen to an operational temperature of 160K.

#### 3.2.2 Filters

The Mercator observatory uses the Geneva photometric system [11]. This is a 7 band photometric system developed at the Geneva Observatory in Switzerland. The 7 filters are indicated with U, B<sub>1</sub>, B, B<sub>2</sub>, V<sub>1</sub>, V and G. In public observations these capitals denote the colours in the Geneva system. Such a colour is defined as:

$$X_{\text{Geneva}} = m_X - m_B \quad \text{for} \quad X = U, V, B_1, B_2, V_1, G. \quad (7)$$



Size of the chip	27.65 mm $\times$ 27.65 mm
Pixel size	13.5 $\mu$ m
Number of pixels	2048 $\times$ 2048
Field of view	6.5' $\times$ 6.5'
Resolution	0.19"/pixel or 5.3 pixels/''
Read out noise	3 electrons RMS at slow pixel rate.

Table 1: Technical specifications of the MEROPE CCD camera.

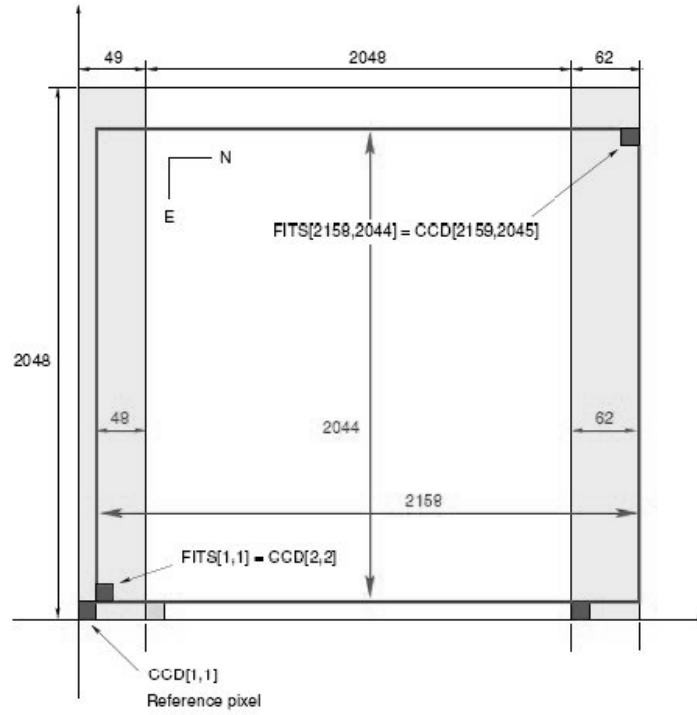


Figure 2: Geometry of the CCD chip. The light grey areas on the sides are the overscan strips and the inner dark grey rectangle corresponds to a 'full-chip' read-out.

These letters represent colours and not observed magnitudes in the filter as is commonly used, for example in the Johnson system. In the rest of the paper we will denote the Geneva filters with an extra "G" (*UG* for example) for clarity.

The filters in the Mercator telescope are Geneva filters except the *IC* and *RG* filters. The *RG* filter is an own filter which is similar to the Johnson R filter, the *IC* filter is from the Cousins filter system. The *VG* transmission curve of the Geneva filter is the same as the V transmission curve of the Johnson system. In table 2 the transmission coefficients and the width are listed. The transmission curves of the filters we used are also plotted in figure 3.

Band	Effective wavelength (nm)		Width (nm)	
Filter	Telescope	Johnson	Telescope	Johnson
U	342.16	365	16.08	68
B1	398.22	-	16.63	-
B	420.09	440	28.12	98
B2	447.76	-	13.88	-
V1	539.56	-	21.22	-
V	548.26	550	28.62	89
G	576.59	-	22.18	-
R	662.91	700	31.38	220
I	749.18	900	23.05	240

Table 2: Transmission coefficients of the filters at the telescope compared to the Johnson photometric system.

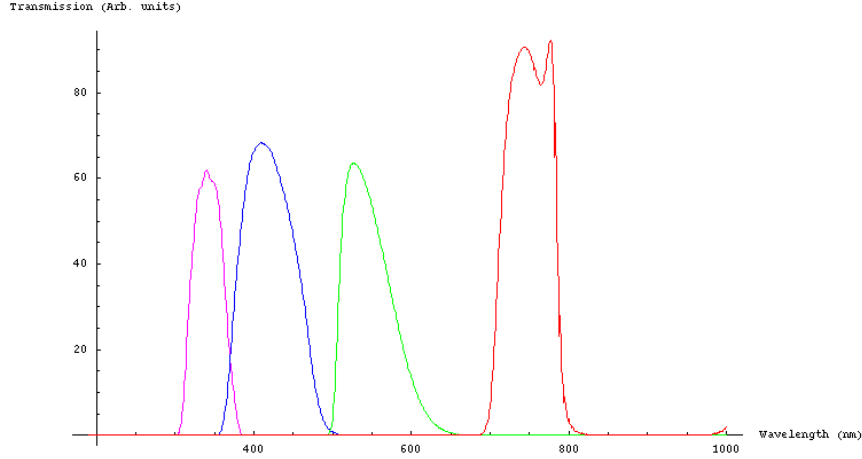


Figure 3: The filters used in our observations. From left to right *UG* (violet), *BG* (blue), *VG* (green) and *IC* (red).

### 3.3 Data collected

Over three observing nights we took images of the galaxy NGC 1073 in 4 filters. We chose the filters in such a way that they would provide information on the slopes of the spectrum of the galaxy in the spots where model data predicted the largest changes for different ages of stellar populations. We ended up using the following filters: *UG*, *BG*, *VG* and *IC*. Table 3 shows the images we've taken and their exposure times, note this table also contains our standards and some images of NGC 884 that were

used for calibration purposes.

### 3.4 Conditions

The first observing night (2005-10-28 to 2005-10-29) our observations were done at a outside temperature of about 8.6 degrees Celsius and a humidity of about 50%. Due to software trouble we've not been able to take flatfields at the beginning of the night. At the end of the night were not able to take a flatfield in the *BG* filter. The second night (2005-10-30 to 2005-10-31) the observation conditions were misarable because of clouds in the sky, all exposures that night failed because of them. The third night (2005-11-01 to 2005-11-02) was nice, flatfields were taken at both the beginning and the end of the night. The images taken of NGC 1073 were fine. The last night (2005-11-02 to 2005-11-03) was also fine, flatfields were taken at both the beginning and the end of the night. Observations of NGC 1073 also turned out fine.

### 3.5 Data reduction and calibrations

For all the images taken of NGC 1073 we went through the following steps: bias subtraction, flatfielding, aligning and calibration.

The Merope CCD sensor has so called overscan regions that are used to correct for bias and dark current. The bias is a base voltage used within the electronics of the CCD to make sure that the amplifiers and analog to digital converters (ADC) that are used during readout function correctly. The bias shows up in every image taken with the CCD as extra counts. The dark current consists of noise electrons that are caught withing the charge collecting areas of a CCD during the exposure. The longer one exposes the more dark current is collected in the resulting image. The dark current is suppressed by cooling the CCD. An overscan region is a region on a CCD that is not exposed to light but that is read out each time the CCD is read out. The overscan region contains both the bias and the dark current counts. The first few columns and the last few columns of the CCD are the overscan area (see image 2).

By fitting a function along these columns and subtracting it from the image it is possible to remove the dark current and bias counts from the image. The assumption being made is that the bias and dark counts are constant along lines within the image. This is reasonable assumption because the images are read out on a line by line basis. Compared to taking bias and dark frames the overscan region method has the advantage of taking into account information on the bias structure and dark current for each exposure and also of saving telescope time by not having to produce bias and dark frames. (Dark frames are made by reading out a CCD after some time but without exposing the CCD to light, bias frames are made by reading out a CCD after zero seconds and without exposing the CCD to light.) The bias and dark current subtraction was performed using the `colbias` package of the IRAF data reduction software. This package uses the overscan region of an image to find the

Sequence	Object	Filter	Exposure time	Universal Time	Airmass	Focus*
039344	NGC 1073	<i>BG</i>	180 s	2005-10-29 03:33:02.79	1.32	1.33
039345	HD 25329	<i>BG</i>	5 s	2005-10-29 03:37:37.08	1.02	
039346	HD 25329	<i>BG</i>	9 s	2005-10-29 03:38:16.10	1.02	
039348	HD 25329	<i>IC</i>	5 s	2005-10-29 03:39:35.30	1.02	
039353	NGC 1073	<i>VG</i>	180 s	2005-10-29 04:08:46.27	1.50	
039354	NGC 1073	<i>IC</i>	250 s	2005-10-29 04:13:04.90	1.53	
039355	HD 27674	<i>VG</i>	5 s	2005-10-29 04:18:45.27	1.29	
039356	HD 27674	<i>BG</i>	10 s	2005-10-29 04:19:23.37	1.29	
039358	HD 27674	<i>IC</i>	5 s	2005-10-29 04:20:48.07	1.29	
039412	Flatfield	<i>IC</i>	130 s	2005-10-29 06:48:19.40		
039413	Flatfield	<i>VG</i>	55 s	2005-10-29 06:52:28.31		
039598	Flatfield	<i>UG</i>	20 s	2005-11-01 18:39:35.93		1.04
039599	Flatfield	<i>BG</i>	20 s	2005-11-01 18:47:11.82		
030600	Flatfield	<i>VG</i>	57 s	2005-11-01 18:49:26.53		
030601	Flatfield	<i>IC</i>	80 s	2005-11-01 18:52:17.68		
039714	NGC 1073	<i>UG</i>	449 s	2005-11-01 23:45:32.98	1.19	
039715	NGC 1073	<i>UG</i>	450 s	2005-11-01 23:54:22.53	1.17	
039716	NGC 1073	<i>BG</i>	270 s	2005-11-02 00:03:43.93	1.15	
039717	NGC 1073	<i>BG</i>	270 s	2005-11-02 00:09:33.46	1.14	
039718	NGC 1073	<i>VG</i>	270 s	2005-11-02 00:15:24.46	1.14	
039719	NGC 1073	<i>VG</i>	270 s	2005-11-02 00:21:13.23	1.13	
039720	NGC 1073	<i>IC</i>	150 s	2005-11-02 00:27:02.68	1.14	1.06
039721	NGC 1073	<i>IC</i>	150 s	2005-11-02 00:30:52.57	1.14	
039722	NGC 1073	<i>IC</i>	150 s	2005-11-02 00:34:41.14	1.13	
039723	NGC 1073	<i>IC</i>	150 s	2005-11-02 00:38:30.34	1.13	
039724	NGC 1073	<i>IC</i>	150 s	2005-11-02 00:42:19.65	1.13	
039725	NGC 1073	<i>IC</i>	150 s	2005-11-02 00:46:07.74	1.13	
039736	NGC 884	<i>UG</i>	92 s	2005-11-02 01:59:35.61	1.16	
039737	NGC 884	<i>BG</i>	20 s	2005-11-02 02:02:57.64	1.17	
039738	NGC 884	<i>VG</i>	10 s	2005-11-02 02:04:47.09	1.17	
039739	NGC 884	<i>IC</i>	9 s	2005-11-02 02:06:25.59	1.17	
039846	Flatfield	<i>IC</i>	105 s	2005-11-02 06:52:18.70		1.07
039847	Flatfield	<i>VG</i>	55 s	2005-11-02 06:56:02.95		
039849	Flatfield	<i>UG</i>	77 s	2005-11-02 07:00:19.09		
039850	Flatfield	<i>VG</i>	20 s	2005-11-02 18:38:51.29		
039851	Flatfield	<i>BG</i>	20 s	2005-11-02 18:46:25.94		
039852	Flatfield	<i>VG</i>	56 s	2005-11-02 18:48:40.82		
039853	Flatfield	<i>IC</i>	92 s	2005-11-02 18:51:31.83		
040114	NGC 884	<i>UG</i>	46 s	2005-11-03 03:17:32.92	1.28	
040115	NGC 884	<i>BG</i>	9 s	2005-11-03 03:19:45.57	1.29	
040116	NGC 884	<i>VG</i>	7 s	2005-11-03 03:21:23.02	1.29	
040117	NGC 884	<i>IC</i>	6 s	2005-11-03 03:22:57.75	1.30	1.07
040124	NGC 1073	<i>UG</i>	450 s	2005-11-03 04:07:28.19	1.64	
040125	NGC 1073	<i>UG</i>	449 s	2005-11-03 04:16:19.67	1.70	
040126	NGC 1073	<i>BG</i>	270 s	2005-11-03 04:25:10.84	1.76	
040127	NGC 1073	<i>BG</i>	270 s	2005-11-03 04:31:00.97	1.84	
040128	NGC 1073	<i>VG</i>	270 s	2005-11-03 04:36:50.99	1.89	
040129	NGC 1073	<i>VG</i>	271 s	2005-11-03 04:42:41.67	1.95	
040130	NGC 1073	<i>IC</i>	150 s	2005-11-03 04:48:33.04	2.00	
040131	NGC 1073	<i>IC</i>	150 s	2005-11-03 04:52:23.07	2.02	
040132	NGC 1073	<i>IC</i>	150 s	2005-11-03 04:56:13.52	2.06	
040133	NGC 1073	<i>IC</i>	150 s	2005-11-03 05:00:45.98	2.11	2.33
040134	NGC 1073	<i>IC</i>	150 s	2005-11-03 05:05:06.25	2.25	
040135	NGC 1073	<i>IC</i>	150 s	2005-11-03 05:08:56.04	2.33	
040153	Flatfield	<i>IC</i>	64 s	2005-11-03 06:55:31.97		
040154	Flatfield	<i>VG</i>	33 s	2005-11-03 06:58:54.49		
040156	Flatfield	<i>VG</i>	40 s	2005-11-03 07:03:49.24		

Table 3: List of exposures, the “Focus” column gives the seeing from the most recent focus star measurement.

bias structure and subtract that from the image.

Before moving on to the flatfielding of our images we masked out a column from the images that had an overexposed stripe in it because of a bad pixel in the Merope CCD. The mask uses a linear interpolation over nearest known good pixels to overwrite the bad pixel data in the stripe.

Flatfields at the Mercator telescopes are so called sky flats, images taken of the twilight sky. The flatfields should be made using a featureless region of the sky (or some other a spatially homogeneous light source). The structure in a flatfield image is then caused by local differences in CCD sensitivity and imperfections in the optics of the telescope and its filters. One can then divide out the differences in sensitivity caused by the CCD, telescope and filters. The flatfields we used were the flatfields taken at the same day the images were taken. For days that had two flatfields available we combined them. The first observing night had no *BG* filter flatfield available so we used the *BG* flatfields from the third night to perform the flatfield correction.

We aligned our images of NGC 1073 using the Karmasutra program. We have not calibrated images of NGC 1073 to the WCS system since we are not in the business of astrometry. We did calibrate the NGC 884 images to the WCS system to aid in the identification of the stars within that cluster using the “wcstool” program. For the images of the first night we had exposures of Geneva standard stars HD25329 and HD27674 available to do calibrations. For the other two nights we had no standard stars so we had to use images of the NGC 884 star cluster which also contain stars with known magnitudes. The standard stars allowed us to find the absorption coefficient values for the atmosphere, we used a standard value of the absorption coefficient for our *IC* band images. The  $\kappa$  values let us correct the images for the atmosphere of the earth. We then used zeropoints of the magnitude scale relevant to the Merope CCD to find absolute values for our photometry.

Because of time constraints we did not look for cosmic ray hits in all our flatfields and images. However, since we did have several exposures of NGC 1073 in each band we did combine the images using the average and using the average sigma clipping algorithm of the IRAF `imcombine` task.

Before doing any photometry on our galaxy we have also subtracted the sky background. This has been done by measuring the average number of counts per pixel per second in four  $100 \times 100$  pixel squares, each 100 pixels from the corner. Assuming a constant background you can subtract the background by subtracting the average value of the four boxes.

We constructed the usual images in counts per second and used the `qphot` task of IRAF to find the magnitudes of the objects in our frame for the standard stars. For our galaxy we defined a few regions that were on the bar and on the spiral arms. For each region we added up all the counts and calculated a magnitude per square arcsecond. We also constructed images that for lack of better words we call magnitude images. These images are calibrated in such a way that they contain magnitude information for each pixel. From those magnitude images we also constructed colour images — colour in the magnitude for one filter minus the magnitude for another

filter sense of the word. Although the magnitude and colour images are somewhat hard to interpret, they do show clearly where the object one observes has a red or blue excess.

## 4 Results

In this section we present the results from 1h46m10.5s integration time. We combined all the images into four images, one for each filter. From these images we made “colour images”, two magnitude images subtracted from each other. We found that this image is quite useful.

We also did photometry on sections of our galaxy. On pages 19 and 20 are the images in all the filters. Indicated with boxes are the areas we used for photometry.

### 4.1 Quantitative data form the galaxy

We have determined the magnitudes and colours from eight areas in the galaxy. The areas consists of 441 pixels, the given value is the result of summing those pixels. The areas we used can be found in the images 4, 5, 6 and 7.

To calculate the error, we used the following formula:

$$\frac{\Delta M}{\Delta F} = \frac{\Delta(2.5 \log F)}{\Delta F} = \frac{\Delta F}{F} \quad (8)$$

In this formula the  $\Delta F$  is the error in counts per second per area. This error comes from noise in the images, uncertainties in calculating the absorption coefficients and subtraction of background level.

The noise uncertainty is calculated by using the standard deviation from the mean value for each area of each pixel, divided by the square root of the number of pixels. The uncertainty in the absorption coefficients is due to uncertainties in calibrating using the standard stars. These uncertainties differ per filter, per night and time of the night, but average to around a few centimagnitudes in the calibration of the standard stars. They are a result of errors in the aperture used in doing photometry with `qphot`. This result for the uncertainty in the absorption coefficient is the standard star calibration error divided by its airmass. The result for calibrating our images using the airmass will then be of the same order as the noise, at the centimagnitude level.

Another error due to airmass correction is due to the ever changing atmosphere. We have taken standard star measurements close to the observing time of our object, but nevertheless the atmosphere can change in this period. This is even more true as we did not have photometric nights. Also, our standards were not taken at the same airmass. The first night we tried to be close, which proved difficult because of the lack of good standard stars. The last two nights we were lucky to be able to use measurements on NGC 884 so airmass was our least worry here. To give an estimate of the errors we present the range of the measurements on standard stars in table 4. Note that on the final two days all the standards were on the same frame! There’s also an uncertainty in the catalogued value of these stars, but these are well below the errors we’ve made so they can be neglected safely.

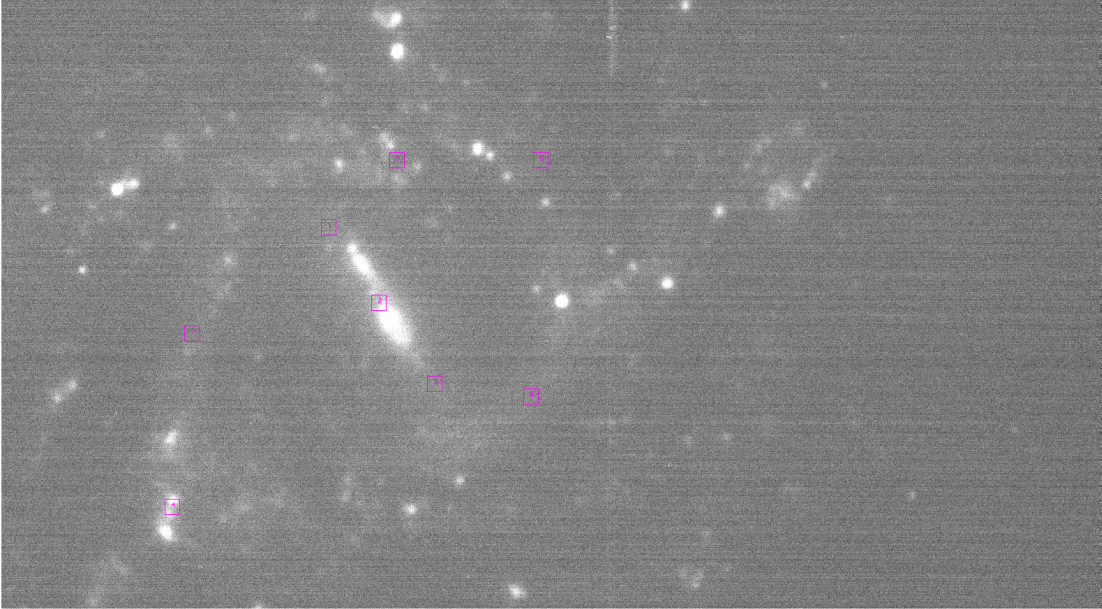


Figure 4: NGC 1073 in the  $UG$  filter. Overlaid are the areas used for photometry.

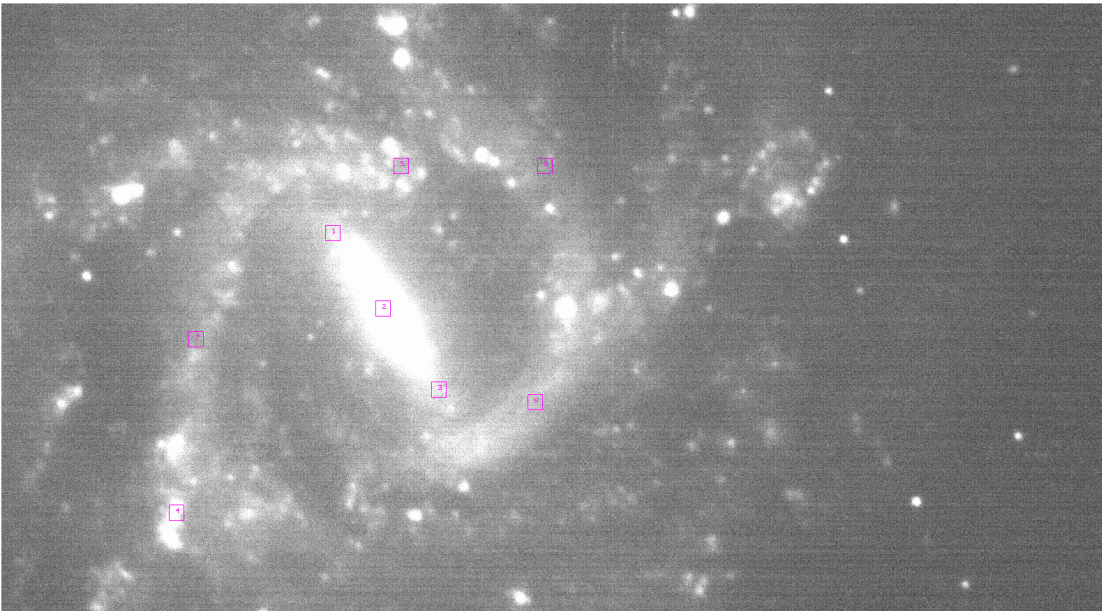


Figure 5: NGC 1073 in the  $BG$  filter. Overlaid are the areas used for photometry.



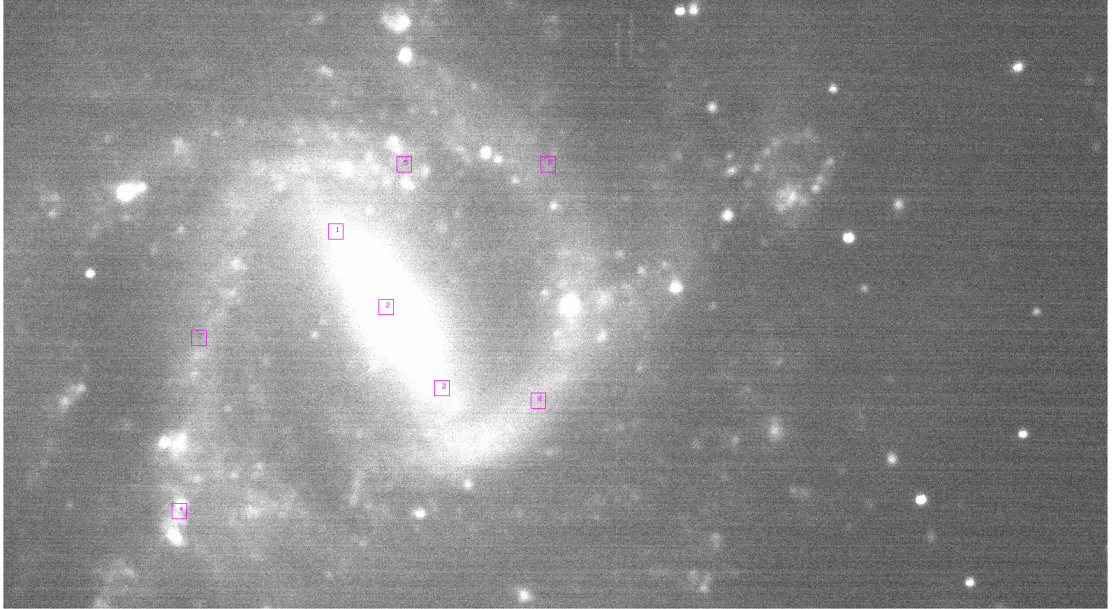


Figure 6: NGC 1073 in the *VG* filter. Overlaid are the areas used for photometry.

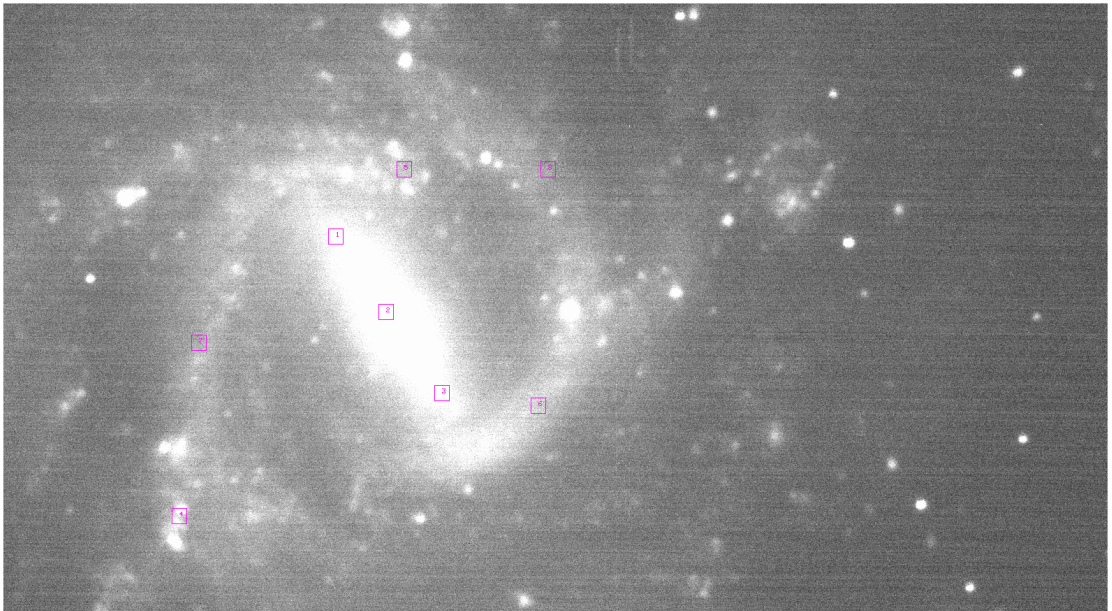


Figure 7: NGC 1073 in the *IC* filter. Overlaid are the areas used for photometry.

Filter	Night	Measurements	Range
BG	2005-10-28	2	$4.5 \times 10^{-2}$
VG	2005-10-28	2	$2.2 \times 10^{-2}$
UG	2005-11-01	3*	$1.6 \times 10^{-1}$
BG	2005-11-01	3*	$7.3 \times 10^{-2}$
VG	2005-11-01	3*	$4.6 \times 10^{-2}$
UG	2005-11-02	3*	$1.4 \times 10^{-1}$
BG	2005-11-02	3*	$7.4 \times 10^{-2}$
VG	2005-11-02	3*	$3.0 \times 10^{-2}$

Table 4: Ranges in the measurements of standard stars. The measurements with an asterisk are from the same frame.

Finally there is an uncertainty in the removal of an average background. We assumed a constant background, which we determined by averaging the value of four  $100 \times 100$  boxes 100 pixels from each corner. Assuming that we're not further off than 5 pixels in each image, the resulting error per image is then 5 divided by the integration time. As we probably have a similar chance of making a too low as a too high estimate of the background, the error is further reduced as we sum the images, by the square root of the number of images. The resulting error per filter can be found in table 5. It can be seen that these errors are very small. They still need to

Filter	Error (Counts s <sup>-1</sup> )
UG	$5.6 \times 10^{-3}$
BG	$8.8 \times 10^{-3}$
VG	$8.7 \times 10^{-3}$
IC	$8.8 \times 10^{-3}$

Table 5: Possible errors due to background subtraction.

be divided by the actual value of the measurements, so these problems give rise to errors of about 1 millimagnitude. Therefore, we have neglected these errors.

Using the `imstat` program from IRAF, we found values for the magnitudes. These values are printed in table 6, still not converted to the Geneva system (hence the subscript “m”). In the brackets are the errors.

Using these numbers, it's an easy exercise to calculate the Geneva colours. They are printed in table 7. Remember that in the Geneva system the difference to the *BG* filter is given. The *IC* – *VG* colour is calculated by subtracting  $VG_m$  from  $IC_m$ , so this colour is not with respect to *BG*.

Area	$UG_m$	$BG_m$	$VG_m$	$IC_m$
1	22.56(8)	21.319(20)	21.470(15)	20.308(13)
2	21.24(5)	20.07(4)	20.33(3)	19.215(26)
3	22.71(9)	21.379(22)	21.462(15)	20.301(12)
4	21.22(6)	20.84(5)	21.73(4)	20.85(3)
5	22.83(12)	21.745(25)	22.129(24)	21.095(21)
6	23.05(13)	21.718(25)	22.006(22)	20.965(19)
7	23.20(15)	22.06(3)	22.434(29)	21.319(23)
8	23.29(17)	22.24(4)	22.61(3)	21.59(3)

Table 6: Magnitudes of the different areas as in figures 4, 5, 6 and 7 and their respective errors due to noise.

Area	$UG$	$VG$	$V - I$
1	1.24(9)	0.151(25)	1.163(20)
2	1.16(7)	0.25(5)	1.11(4)
3	1.33(10)	0.083(26)	1.161(20)
4	0.38(8)	0.89(7)	0.88(6)
5	1.09(12)	0.38(3)	1.03(3)
6	1.33(13)	0.29(3)	1.041(29)
7	1.14(15)	0.38(4)	1.11(4)
8	1.05(17)	0.36(5)	1.02(5)

Table 7: Colours of the different areas in figures 4, 5, 6 and 7.

## 4.2 Images

We found that it is useful to make “colour” images. This is an image with in each point the value of a colour. Figure 8 is the  $UG - IC$  colour image. This image spans the largest band, thus showing best where hot and cold patches are. In figure 9 you can find the  $BG - IC$  colour image, and in figure 10 the  $V - I$  image. Also included is the  $UG - BG$  image (figure 11). This image shows places where you can find the very hot stars. It is therefore a good indicator of star formation

## 4.3 Description of observations

In this section we will discuss counts per second per pixel a lot. Therefore, we will stick here to this definition: bright means a high number of counts per second per pixel, faint a low number of counts.

As is mentioned before we have images taken using the  $UG$ ,  $BG$ ,  $VG$  and  $IC$  filters. Our images show the barred spiral galaxy NGC 1073. There is some separation



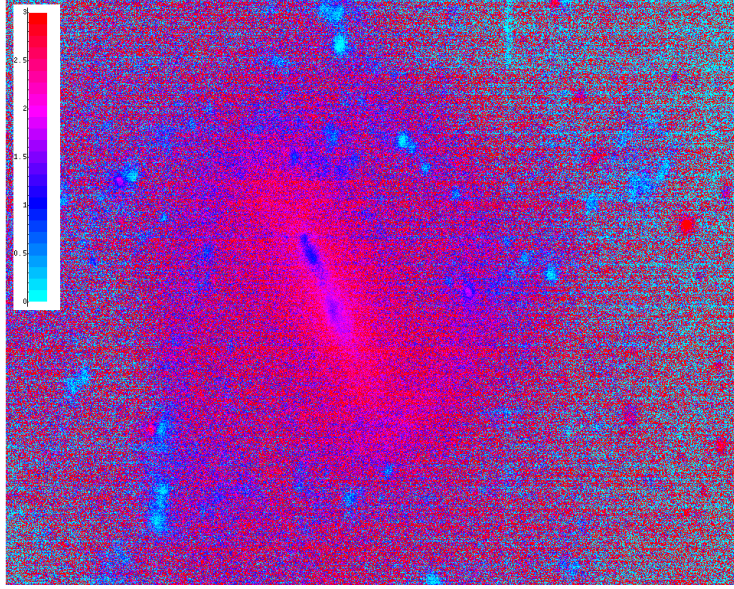


Figure 8: The  $UG - IC$  colour image.

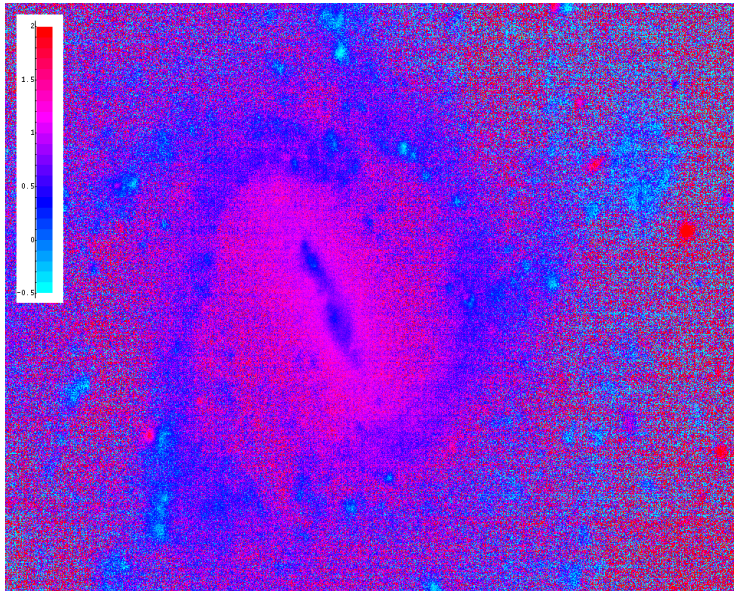


Figure 9: The  $VG - IC$  colour image.



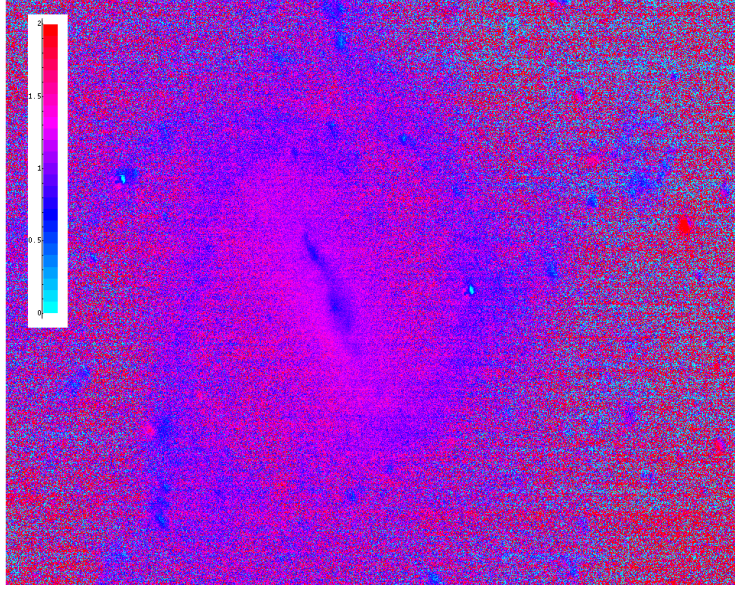


Figure 10: The  $BG - IC$  colour image.

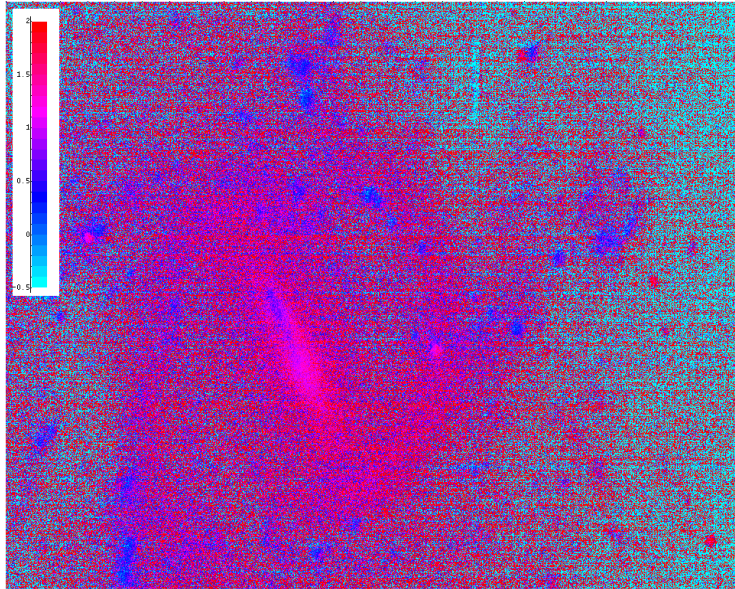


Figure 11: The  $UG - BG$  colour image.

of the bar and the spiral arms, especially in the short wavelength images. In the  $BG$  image the spiral arms are more defined than in the rest of the filters. We have a low brightness in the  $UG$  band, compared to the other bands. The bar is brightest in the  $IC$  band, again compared to the other bands.

There is a bright patch in all the filters in the lower left part of the galaxy (around area number 4). To the right of the galaxy there is a roughly circular shaped patch, which is quite blue, that seems connected to the galaxy. Maybe it is a satellite galaxy. Some of the images show remnants of the stripe caused by the bad pixel in the CCD. This stripe is to the right part of the galaxy going from top to bottom, but it is most prominent near the top of the galaxy. We have tried to remove this bad pixel, what you see here is the still visible remnant. The lumpy nature of the spiral arms is less pronounced in the  $IC$  filter than in the  $BG$  filter. Looking at the  $BG - IC$  colour image, we see that stars around the galaxy are redder than the galaxy itself.

In the middle of the right part of the galaxy there is a really bright source in all filters. This is clearly seen in the RGB colour picture on the cover. The source is pretty blue so if it were to be a foreground star we would be dealing with an O or B star. The change of this object being a such a star is really small, since we are observing far from the galactic plane. As the scale height of O stars is small, there are no O stars expected in the line of sight to NGC 1073. In the immediate surroundings there is also a super nova remnant 1962L, according to SIMBAD. This also cannot be the explanation, since this supernova went of a long time ago and should be very faint now. There are also quasars near our galaxy, but according to SIMBAD not in that spot. There is another such source to the upper left of our galaxy, for which we also do not have an explanation. Another remark is that these objects seem less blue than area 4, which we identify as an area of active star formation.

From the raw data (tables 6 and 7) it is clear that area 4 has different colour than all other areas. This can also be seen from the colour images. We think this is a region of active star formation. Area 5 lies also in such a region, at least if we look at the colour images and the  $UG$  and  $BG$  images we see a bright area at short wavelengths. This is not shown in the colours in table 7. Close inspection shows that we managed to place this area exactly in between two bright spots, so maybe we missed the area of active star formation.

Again looking at the data in table 7, there is some evidence that the spiral arms are bluer than the bar. This is most prominent in the  $IC - VG$  and  $VG$  colour. The colour images support this belief. That this difference is not so prominent in the  $UG$  colour, except for area 4, can be explained by realising that the stars with a very blue spectrum are only found close to stellar nurseries. Assuming that area 4 is such an area, it is expected that those stars can be found only there.

From the  $UG - IC$  image (figure 8) and the  $UG$  image itself (figure 4) it can be seen that the bar is not symmetric. This feature becomes less prominent at longer wavelengths, as can be seen in the  $BG - IC$  and  $VG - IC$  images. It is bluer above the middle than below. It is interesting to note that close to the bar in the spiral arms (near area 5) there's also a blue patch of the spiral arms. This suggests some

connection to the asymmetry of the bar with the distribution of blue patches in the spiral arms. Another possibility of this asymmetry lies in the distribution of dust. If there's more dust in the lower part of the bar, you would expect more extinction there, especially in the short wavelengths. However, this view contradicts the common belief that the central areas of a spiral galaxy are relatively poor in dust.

#### 4.4 Comparing colours to the Starburst99 model

In this section we compare our observations against the theoretical results of the Starburst99 model. We only look at instantaneous formation evolution, thus looking at the evolution of a group of stars formed at the same moment. The model is run for metallicity  $Z = 0.020$  and a Salpeter IMF (equation 1). We used this metallicity as we found one reference where for NGC 1073 a metallicity of  $Z = 0.019$  is used[6]. Examples of results from the Starburst99 model can be found in figure 1. We calculated colours from the resulting spectra, using a program to calculate the convolution integral of these spectra and filter transmission data (see equation 5 and 6). We calibrated this data by subtracting the convolution integral over the Kurucz spectrum of Vega, and adding to the  $UG$  and  $VG$  the Geneva colours of Vega. As Vega is used for calibrating absolute photometry, the  $V - I$  colour of Vega is defined to be zero.

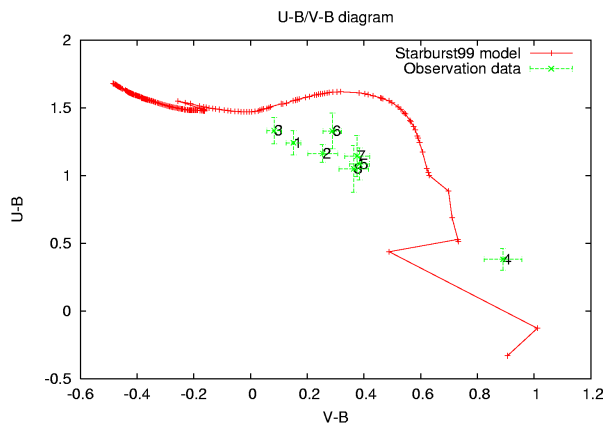


Figure 12: Plot of  $UG$  against  $VG$ .

In figure 12 you find the results from the Starburst99 model, in the  $UG$  against  $VG$  colour. Note that in this figure we indicated this as  $U - B$  and  $V - B$ . This image clearly shows the difference between area 4 and the other areas. This is what we expected since we identified area 4 as an area of active star formation. Using the raw data of the simulation we can also infer a single starburst age for each area. Area 4 lies close to the model near points with ages of an order of magnitude of 10 million years. The area furthest to the left (area 3) compares to an age of a little

over one billion years (1.1 to 1.2 billion years). The spiral arm areas without active star formation (areas 5 to 8) roughly coincide with ages of about 500 million years, the bar areas (1 to 3) seem a little older with ages of around 700 million years.

Note that all the older areas are below the model points. This can be explained by realising that this data is for an instantaneous star formation. Continuous star formation requires an appropriate linear combination of all the points in the model, and can therefore fit the observations better. However, given the few filters, this procedure would be highly questionable. Also realize that this model is only for one metallicity. Maybe other metallicities fit the observations better.

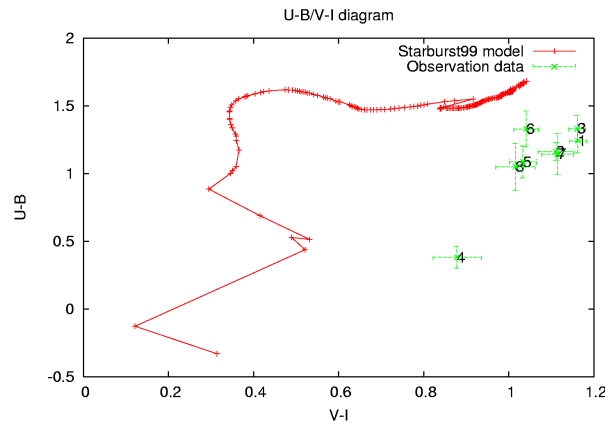


Figure 13: Plot of  $UG$  against  $V - I$ .

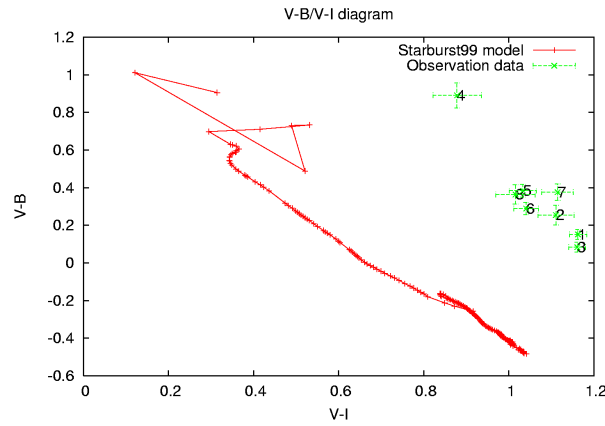


Figure 14: Plot of  $VG$  against  $V - I$ .

The plots of  $UG$  and  $VG$  against  $V - I$  (figures 13 and 14) both show a large difference between observations and model data points. We note that if you shift the



$V - I$  colour of the model about 0.5 to the right, you would get reasonably close to the observation. We think this error is due to an error in calculating the  $V - I$  colour. It is calculated by subtracting from  $VG_m$  the  $IC$  filter, under the assumption that  $VG_m \equiv V_{\text{Johnson}}$ . Probably this assumption fails, giving a  $V - I$  colour to Vega and thus ruining our  $V - I$  colour. If we do make the suggested shift of 0.5, the areas match the model points at similar ages as seen in the  $UG$  against  $VG$  plot of figure 12. We again note that area 4 is in a completely different part in these graphs. Furthermore, the bar areas (1 to 3) are close together, as are the spiral arm areas without active star formation (5 to 8). There seems to be a small gap between the spiral arm areas and the bar areas. However, we cannot quantify this claim as the errors are too large.

## 5 Conclusions

We have found that the spiral arms of NGC 1073 are bluer than the bar. The spiral arms have a lumpy appearance, especially in the short wavelengths. A good explanation for this lumpy appearance is that it is caused by localised star formation. Noting that this structure can only be found in the spiral arms, this is evidence that star formation occurs in the spiral arms. This is in agreement with the theory of galaxy evolution.

We also found aspects we didn't understand. The bar is not symmetric in the short wavelength images, for which we have no particular explanation. We also found two very bright point sources, of which we do not know what they are.

Comparing the results to the Starburst99 model, we found that the  $UG$  against  $VG$  plot (figure 12) gave a reasonable resemblance between model and observations. Area 4 stood out as clearly different in these plots. Ages found by assuming instantaneous star formation histories were also reasonable and suggested that the bar is on average somewhat older than the spiral arms. The plots of  $UG$  and  $VG$  against  $V - I$  (figures 13 and 14) showed a large discrepancy between the model and the observations. A possible explanation is that the  $V - I$  colour is computed incorrectly for the model. Assuming that this is the case, we found similar ages for all colours.

## 6 Discussion

The conclusion that the spiral arms are bluer than the central bar are supported by the colours in table 7. The indicated errors are smaller than the differences in these colours. In these errors the airmass correction is not included. This is not justified, especially since we didn't have photometric nights. We have indicated the spread in the extinction coefficients as obtained from the standards. These numbers suggest an error similar to the error due to noise, which is indicated in the table. As the difference in colours is quite a bit larger than these errors, we think we can still hold this claim if we include these errors.

That the colours of area 4 are different is beyond any doubt. The differences are of order  $10\sigma$ , and will be off by orders of  $\sigma$  after including errors in airmass calibration.

The airmass calibration should have affected all the measurements in one filter similarly, as we corrected all pixels by the same number. Thus errors in airmass correction may lead to wrong colours, they do not reduce the gap between two sources in the same colour. This also means that differences in colour remain the same. Realising this further supports our claims.

The airmass correction would have been much better if we had more sources on different airmasses. This would have allowed us to reconstruct the atmosphere during the night, thereby having a much better idea of which extinction coefficient to use. The first day we had two standard stars. Although they provided accurate data, the airmasses were quite different from NGC 1073. This is due to the lack of standards in the Geneva system.

The second and third night NGC 1073 was observed, we had no data from standard stars. We used an exposure of NGC 884, which contains stars with known Geneva colours to calibrate it. However, as this is only one frame, it is impossible to reconstruct the behaviour of the extinction coefficients at different airmass.

Finally, we corrected for the airmass in the *IC* filter by using a standard airmass. This because we had no data of our standard stars in the *IC* filter. However, this correction is very small, as the atmosphere is very transparent to light passing this filter. The resulting error is thus also small.

We corrected for a bad pixel on the CCD. This has not affected the data provided, as this bad pixel did not occur in areas we used to calculate the colours. We corrected for this pixel because it made the automatic scaling of the pictures better, and to avoid the large number of stripes in our picture we would get from adding images.

We did not correct for the intergalactic extinction and the extinction in our Milky Way. We did not correct for intergalactic extinction because it's almost impossible to do. Correcting for extinction in the Milky Way was not really necessary, as we were looking away from the galactic plane.

Comparing the observations with Starburst99 model data, we found that the diagrams in which *UG* and *VG* were plotted against  $V - I$  (figures 13 and 14) were shifted. We believe it is an error in  $V - I$ , since the diagram showing *UG* against

$VG$  (figure 12) seems reasonable. This suggests that the  $UG$  and  $VG$  colours are computed correctly, leaving the error to  $V - I$ .

## List of Tables

1	Technical specifications of the MEROPE CCD camera. . . . .	12
2	Filter transmission curves . . . . .	13
3	List of exposures . . . . .	15
4	Standard star calibration errors . . . . .	21
5	Errors in background subtraction . . . . .	21
6	Magnitudes of area's in NGC 1073 . . . . .	22
7	Colours of areas in NGC 1073 . . . . .	22

## List of Figures

1	Synthetic stellar population spectra . . . . .	9
2	CCD chip layout . . . . .	12
3	Transmission curves . . . . .	13
4	NGC 1073 in the <i>UG</i> filter . . . . .	19
5	NGC 1073 in the <i>BG</i> filter . . . . .	19
6	NGC 1073 in the <i>VG</i> filter . . . . .	20
7	NGC 1073 in the <i>IC</i> filter . . . . .	20
8	The <i>UG</i> – <i>IC</i> colour image. . . . .	23
9	The <i>VG</i> – <i>IC</i> colour image. . . . .	23
10	The <i>BG</i> – <i>IC</i> colour image. . . . .	24
11	The <i>UG</i> – <i>BG</i> colour image. . . . .	24
12	Plot of <i>UG</i> against <i>VG</i> . . . . .	26
13	Plot of <i>UG</i> against <i>V</i> – <i>I</i> . . . . .	27
14	Plot of <i>VG</i> against <i>V</i> – <i>I</i> . . . . .	27

## References

- [1] E. Bertone, A. Buzzoni, L.H. Rodríguez-Merino, and M. Chávez. Stars at high resolution: a library of synthetic spectra from 850 to 7000 Å. *Memorie della Societa Astronomica Italiana*, 75:158–+, 2004.
- [2] L.M. Close, R. Lenzen, J.C. Guirado, E.L. Nielsen, E.E. Mamajek, W. Brandner, M. Hartung, C. Lidman, and B. Biller. A dynamical calibration of the mass-luminosity relation at very low stellar masses and young ages. *Nature*, 433:286–289, January 2005.
- [3] P. Coelho, B. Barbuy, J. Meléndez, R.P. Schiavon, and B.V. Castilho. A library of high resolution synthetic stellar spectra from 300 nm to 1.8  $\mu$ m with solar and  $\alpha$ -enhanced composition. *A&A*, 443:735–746, November 2005.
- [4] Geert Davignon. <http://www.mercator.iac.es/>, April 2005.

- [5] R.S. Ellis, R.G. Abraham, and M. Dickinson. The Relative Star Formation Histories of Spiral Bulges and Elliptical Galaxies in the Hubble Deep Fields. *ApJ*, 551:111–130, April 2001.
- [6] P. Kaaret. Optical Sources near the Bright X-Ray Source in NGC 1073. *ApJ*, 629:233–238, August 2005.
- [7] D. Kereš, N. Katz, D.H. Weinberg, and R. Davé. How do galaxies get their gas? *MNRAS*, 363:2–28, October 2005.
- [8] M.R. Krumholz and C.F. McKee. A General Theory of Turbulence-regulated Star Formation, from Spirals to Ultraluminous Infrared Galaxies. *ApJ*, 630:250–268, September 2005.
- [9] C. Leitherer, D. Schaerer, J.D. Goldader, R.M.C. Delgado, C. Robert, D.F. Kune, D.F. de Mello, D. Devost, and T.M. Heckman. Starburst99: Synthesis Models for Galaxies with Active Star Formation. *ApJS*, 123:3–40, July 1999.
- [10] L.A. MacArthur, S. Courteau, E. Bell, and J.A. Holtzman. Structure of Disk-dominated Galaxies. II. Color Gradients and Stellar Population Models. *ApJS*, 152:175–199, June 2004.
- [11] F. Rufener and B. Nicolet. A new determination of the Geneva photometric passbands and their absolute calibration. *A&A*, 206:357–374, November 1988.
- [12] E.E. Salpeter. The luminosity function and stellar evolution. *ApJ*, 121:161–+, January 1955.
- [13] M. Sarzi, H.W. Rix, J.C. Shields, L.C. Ho, A.J. Barth, G. Rudnick, A.V. Filippenko, and L.W. Sargent. The Stellar Populations in the Central Parsecs of Galactic Bulges. *ApJ*, 628:169–186, July 2005.
- [14] E.D. Skillman. Star formation histories in local group dwarf galaxies [review article]. *New Astronomy Review*, 49:453–460, November 2005.
- [15] J.M. van der Hulst and R. Sancisi. Gas Accretion in Galactic Disks. In *ASP Conf. Ser. 331: Extra-Planar Gas*, pages 139–+, June 2005.
- [16] C. van’t Veer-Menneret and D. Katz. Grids of ATLAS9 stellar-atmosphere models: colors and synthetic spectra. A critical review. *Journal of Astronomical Data*, 7:8–+, December 2001.
- [17] G.A. Vázquez and C. Leitherer. Optimization of Starburst99 for Intermediate-Age and Old Stellar Populations. *ApJ*, 621:695–717, March 2005.